Electron Paramagnetic Resonance Measurements of Four Nitroxide Probes in Supercooled Water Explained by Molecular Dynamics Simulations

Patrick J. McMillin, Matthew Alegrete, Miroslav Peric, and Tyler Luchko*

Department of Physics and Astronomy, Center for Biological Physics, California State University at Northridge, Northridge, CA 91330, United States

E-mail: tluchko@csun.edu

Abstract

Electron paramagnetic resonance (EPR) measurements of the rotational diffusion of small nitroxide probes have been demonstrated to be a powerful technique for experimentally investigating the properties of supercooled liquids, such as water. However, since only the rotational diffusion of the probe molecules is measured and EPR measurements are indirect, it is not clear what the relationship between the behavior of water and the probe molecule is. To address this, we have performed molecular dynamics simulations of four nitroxide probes in TIP4P-Ew and OPC water models in order to directly compare with EPR experiments, and to determine the behavior of the water and the underlying microscopic coupling between the water and the probes. In all, 200 ns simulations were run for 23 temperatures between 253 K and 283 K for all four probes with each water model for an aggregate of $36.8 \,\mu s$ of simulation time. Simulations for both water models systematically underestimated the rotational diffusion coefficients for both water and probes, though OPC simulations were generally in better agreement with experiment than TIP4P-Ew simulations. Despite this, when the temperature dependence of the data was fit to a power law, fit parameters for TIP4P-Ew were generally in better agreement with experiment than

OPC. For probe molecules, the singular temperature was found to be $T_0 = 226.5 \pm 0.4 \,\mathrm{K}$ from experiment, $T_0 = 208 \pm 2 \,\mathrm{K}$ for OPC water and $T_0 = 215 \pm 2 \,\mathrm{K}$ for TIP4P-Ew water. While for water molecules, the singular temperature was found to be $T_0 = 220.3 \pm 0.2 \,\mathrm{K}$ from experiment, $T_0 = 208 \pm 2 \,\mathrm{K}$ for OPC water and $T_0 = 220 \pm 1 \,\mathrm{K}$ for TIP4P-Ew water. Systematic underestimation of the rotational diffusion coefficients was most pronounced at lower temperatures and was clearly observed in changes to the Arrhenius activation energy. Above the maximum density temperature of $T_{\rho_{\text{max}}} = 277 \,\text{K}$, an activation energy of $E_A \approx 16.7 \,\mathrm{kJ/mol}$ was observed for the probes from experiment, while OPC had $E_A \approx 15.2 \,\mathrm{kJ/mol}$ and TIP4P-Ew had $E_A \approx 14.6 \,\mathrm{kJ/mol}$. Below the maximum density temperature, the activation energy jumped to $E_A \approx 32.5 \,\mathrm{kJ/mol}$ for experiment but only $E_A \approx 23 \, \mathrm{kJ/mol}$ for OPC and $E_A \approx 22 \,\mathrm{kJ/mol}$ for TIP4P-Ew. In all cases, we saw good agreement between the behavior of the probe molecules and water. To understand why, we calculated the average number of hydrogen bonds between the probe molecules and water. From this, we were able to explain the rotational diffusion times for all of the probes. These results show that current molecular models are sufficient to capture physical phenomena observed with EPR and to help elucidate why the probes provide accurate insights to the behavior of supercooled water.

Introduction

Water is very likely the most important biological molecule, without which life would be impossible. 1,2 It is also very important in many industrial processes as a solvent, reactant, product or as an impurity. Water can exist in many different forms of which, for example, 15 are crystalline and three are liquid.³⁻⁵ When water exists in a metastable liquid state below its freezing point it is called supercooled water. In nature, droplets of supercooled water can exist in deep convective clouds at temperatures as low as 235.5 K.⁶ Recently, it has been observed that supercooled water can transiently exist for a few milliseconds down to 227^{+2}_{-1} K.⁷ Interestingly, supercooled water can exist even in many cold-blooded vertebrates, such as reptiles, which can be spontaneously revived upon warming after supercooling to body temperatures as low as -4 °C to -8 °C. 8 In addition, many of peculiar and unusual properties of water are more pronounced in the supercooled region. 7,9-11 Therefore, it is not surprising that supercooled water is one of the most studied forms of water.

Electron paramagnetic resonance (EPR) spectroscopy has been used to study the rotation of nitroxide spin probes in supercooled water. 12-17 The effect of the supercooled water surroundings on the rotation of the small polar spin probe 4-hydroxy- 2,2,6,6tetramethylpiperidine-1-oxyl (TEMPOL) revealed the coexistence of two liquid phases, the Debye-Stokes-Einstein breakdown and the decoupling of the probe's rotation from the viscosity at 225 K. 12 Also, the EPR spectrum of the same probe indicated that supercooled water coexists with cubic ice in the temperature range of $140 - 210 \,\mathrm{K}$. Recently, Peric et al. 18 have used EPR spectroscopy to determine features of the rotation of four small nitroxide spin probes (Figure 1), perdeuterated 4-hydroxy-2,2,6,6-tetramethylpiperidine-1-oxyl (pDTOH or TEM-POL), perdeuterated 2,2,6,6-tetramethylpiperidine-1-oxyl (pDT or TEMPO), perdeuter-

ated 4-oxo-2,2,6,6-tetramethylpiperidine-1-oxyl (pDTO or TEMPONE), and ditertbutyl nitroxide (DTBN). This work has shown that the rotational correlation time of all of the probes decouples from viscosity at 277K. Also, the activation energies of the rotation of the probes and the water viscosity are very close above 277 K, while below 277 K the activation energies of the probes' rotation become greater than the activation energy of water viscosity. Most interestingly, it has been shown that the rotational correlation time of the probes can be fit well to a power law function with a singular temperature of 228 K in the same manner as it has been done in the case of a number of physical properties of water by Speedy and Angell. 19,20

This work has shown a decoupling of rotational diffusion from viscosity around 277 K, as well as a prediction of a singularity at 228 K, an energy barrier which cannot be crossed without the water changing phase and freezing. Later, Peric et al.²¹ extended their work to the translational diffusion of pDTO. In this work, based on the findings of several extensive MD simulations^{20,22–24} that both rotational and translational diffusion of water are affected by the existence of long-lived cages of surrounding water molecules, they hypothesized that a pDTO probe molecule might be trapped in such a cage for some time before it jumps to a next cage. In their next paper 25, using different data analysis, the author did not observe any indication of jump diffusion, which means that the question of translational jump diffusion is still an open question.

The four nitroxide spin probe molecules are often used as "reporters" to study a variety of biological and chemical systems. ²⁶ Also, one of those molecules has recently been used to study the nano-structural organization of room temperature ionic liquids. ²⁷ In the supercooled water study, ¹⁸ the rotational correlation time of pDTOH in water is found to be much slower than the rotational correlation times of the other three spin probes. The difference is explained by the presence of the OH group, which is involved in additional hydrogen bonding. Therefore, to improve the study of differ-

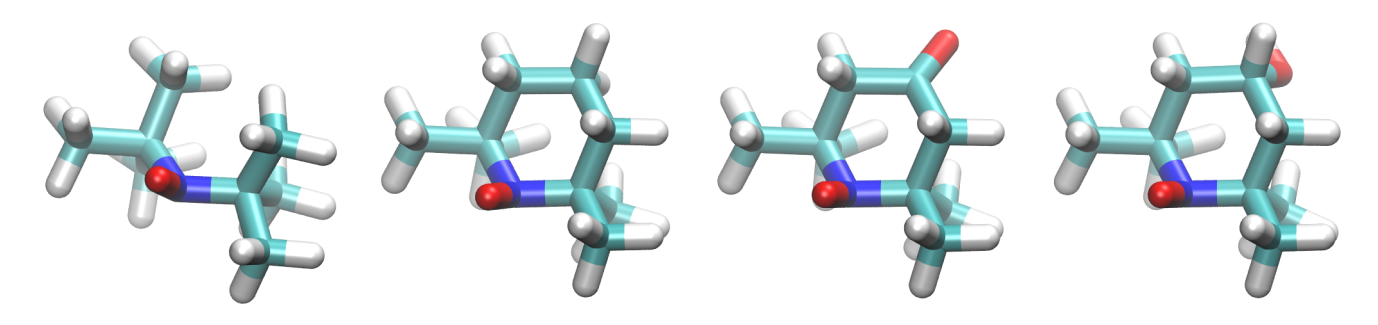


Figure 1: Molecular structure of probe molecules. From left to right: DTBN, pDT, pDTO and pDTOH. Cyan - carbon, blue - nitrogen, red - oxygen, white - hydrogen. Free electrons are located on the oxygen atoms bound to the nitrogen in each probe.

ent biological and chemical systems, it would be beneficial to further our understanding of the interactions of the four spin probes with their surroundings, especially their involvement in hydrogen bonding.

To address the question of rotational diffusion in supercooled water, we have employed classical molecular dynamics of all atom models. Our work here aims to validate simulations against the experimental results of Peric et al. in order to use the simulations to better understand what is physically happening and examine the suitability of these probes to be an accurate representation of water itself. We use analysis techniques available in the AMBER16 molecular dynamics suite ^{28,29} to find rotational diffusion correlation times³⁰ for a range of temperatures between 253 K and 353 K and to compare results to those of Peric et al. The rotational diffusion analysis from Wong and Case has proven to be very useful in analysis of proteins. 31–33 In addition, we also intend to study, in detail, the hydrogen bonding of each spin probe.

Theoretical Methods

Simulations

The MD simulations were performed using the AMBER16 software package. ^{28,29} The antechamber module was used to parameterize the small nitroxide probes (Figure 1) with the generalized Amber force field (GAFF)³⁴ and charges derived from the pyR.E.D. server ^{35–39},

using default settings except for assigning a total charge of 0 and spin multiplicity of 2 for each molecule. The all of hydrogen atoms in the probe molecules were perdeuterated (masses double) to match experiments. Each probe molecule was then solvated in a 25 Å, octahedral, box of either OPC⁴⁰ or TIP4P-Ew⁴¹ water using tleap, followed by 1000 steps of minimization in sander using Limited-Broyden-Fletcher-Goldfarb-Shanno quasi-Newton algorithm 42 via the XMIN module. From this, 23 simulations were prepared with temperatures from 253 K to 353 K in 2 K increments from 253 K to 283 K and in 10 K increments from 283 K to 353 K by heating to their target temperatures and equilibrating over 200 ps using a Langevin thermostat, controlling the pressure using a Monte Carlo barostat with isotropic position scaling. A one step simulation at constant energy and volume was used to remove center of mass drift before starting production runs. The production phase of the simulation consisted of 200 ns of simulation time at constant energy and volume performed with pmemd.cuda 43 with a time step of 0.5 fs and the SHAKE algorithm 44 was used to constrain hydrogen bond lengths. Particle-mesh Ewald summation 45 was used for electrostatics calculations with dsum_tot set to 10^{-7} and a 10 Å cutoff was used for the direct sum part of non-bonded interactions. In order to avoid convergence problems in the diffusion analysis, 5 kcal/mol torsion restraints were added to limit structure changes from the most common chair conformer 46. Coordinates were saved for

analysis once every 2000 frames.

To estimate the numerical error in our simulation protocol, we also carried out a slightly modified protocol for each probe at the highest and lowest temperatures. Rather than selecting the last frame from our pressure and temperature equilibration runs, we calculated the average volume and temperature over the final 150 ps and selected the frame that had the smallest deviation from the averages. We then carried out 10 ps of constant temperature and volume molecular dynamics with motion removal, followed by 200 ns of production runs. From this, we estimated 10% relative error for rotational diffusion correlation coefficients and 1% for the number of hydrogen bonds.

Rotational Diffusion Correlation Time

The cpptraj ⁴⁷ command rotdif ³⁰ was used to analyze rotational diffusion. We used the standard procedure ²⁹, in which, for each frame of the trajectory, a rotation matrix is generated to RMS the solute molecule to an average structure. Then, the rotdif algorithm assigns randomly oriented unit vectors to the solute, which are rotated using the previously calculated rotation matrices and the time correlation function calculated using

$$\langle P_{\ell} \left[\mathbf{n}(0) \cdot \mathbf{n}(\tau) \right] \rangle = \lim_{T \to \infty} \frac{1}{T} \int_{0}^{T} P_{\ell} \left[\mathbf{n}(t) \cdot \mathbf{n}(t - \tau) \right] dt \quad (1)$$

where P_{ℓ} is a Legendre polynomial of order ℓ , T is temperature, t is time, \mathbf{n} is the randomly oriented unit vectors, and τ is the rotational diffusion correlation time. In this work, we have fit the correlation data with a single exponential function, as was done for the nitroxide probe data in Peric et al. 18, though correlation functions can be best fit using multiple exponentials. In this case, integrating the correlation function produces the rotational correlation time,

$$\tau_l(n) = \int_0^\infty d\tau \, \langle P_l \left[\mathbf{n}(0) \cdot \mathbf{n}(\tau) \right] \rangle \qquad (2)$$

for each vector. To improve the numerical integration, cubic splines are applied to smooth the time correlation function. While the diffusion constant can be calculated with full anisotropy, we observed little difference and report the isotropic values. In this work, we used the second order Legendre polynomial, 1000 random vectors oriented using heavy atoms only probe molecules and all atoms for water molecules, and a time step of 1 ps between frames over a window of 5 ns. The final the diffusion constant is then the average of the diffusion constants for the randomly assigned vectors, giving an effective rotational correlation time of the anisotropic diffusional motion. This can be compared with experimental data, which only reports isotropic rotational correlation times.

Rotational diffusion correlation times were calculated for the four nitroxide probes and a randomly selected water from the pDTO simulations for both water models. Correlation times were calculated for each simulation along with the average temperature of the simulation.

Hydrogen Bond Counting

Hydrogen bonds are counted by using the cpptraj command hbond.²⁹ The distance between a donator atom (D) and an acceptor atom (A) is checked, as well as the angle formed between A, the donated hydrogen (H), and D (angle A-H-D). If the A-D distance is less than 3.5 Å, and the A-H-D angle is greater than 145°, then a hydrogen bond is counted. This check is done between all possible donor and acceptor atoms in each frame of the simulation, and then the average number of hydrogen bonds over all frames is computed.

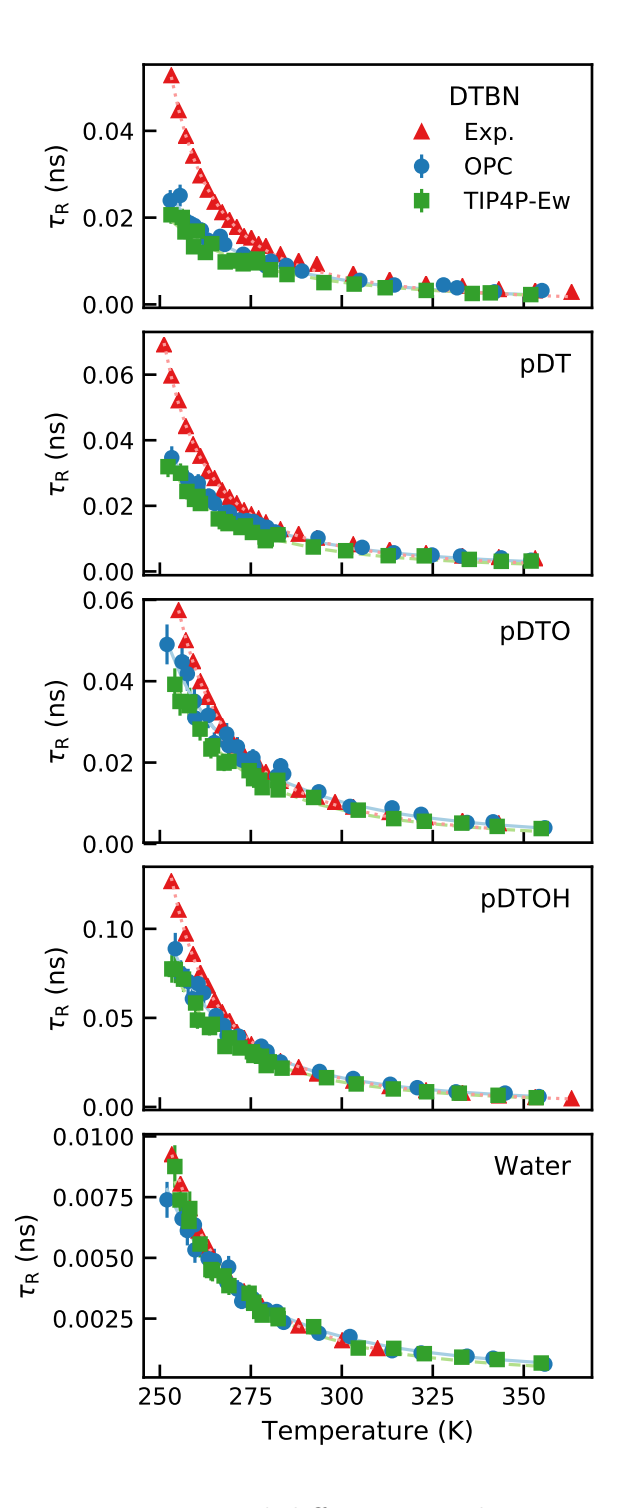


Figure 2: Rotational diffusion correlation time as function of temperature for experiment and OPC and TIP4P-E water models. Data are fit with eq 3 and parameters found in Table 1. Experimental data from ¹⁸.

Results

Power Law Behavior

Table 1: Fit parameters for power law, eq 3, broken up by experiment (top) and simulation (bottom). Standard error in the last digit is given in parentheses. Nitroxide probe and water parameters for experiment are fits to raw data from Peric et al. 18 and Qvist et al. 48.

Probe	T_0 (K)	$\tau_{R0} \; (\mathrm{ps})$	R^2					
Experiment								
DTBN	227.0(4)	0.69(2)	0.9973					
pDT	226.5(3)	0.81(2)	0.9982					
pDTO	224.3(4)	1.08(3)	0.9985					
pDTOH	228.1(3)	1.56(3)	0.9990					
Water	220.3(2)	0.207(2)	0.9999					
OPC								
DTBN	208(3)	1.1(1)	0.9777					
pDT	210(1)	1.42(9)	0.9934					
pDTO	210(2)	2.0(2)	0.9777					
pDTOH	218(2)	2.4(2)	0.9854					
OPC	208(2)	0.35(4)	0.9840					
TIP4P-Ew								
DTBN	208(4)	0.9(2)	0.9586					
pDT	216(2)	0.90(8)	0.9870					
pDTO	214(2)	1.4(1)	0.9882					
pDTOH	220(1)	1.9(2)	0.9887					
TIP4P-Ew	220(1)	0.20(2)	0.9891					

To assess the accuracy of the simulations, we began by comparing the rotational diffusion correlation times over the the entire temperature range (Figure 2), as well as separately considering low $(T < 277 \,\mathrm{K})$ and high (T >277 K) temperatures regimes (Figure 3). In general, nitroxide probe correlation times calculated from simulations are in good agreement with those measured from experiment, though simulations tend to have shorter correlation times, particularly at lower temperatures. The discrepancy is largest for the smallest probes, DTBN and pDT, though calculations for pDTO and pDTOH also underestimate the correlation times. This is true of both water models, though OPC gives values that are slightly higher than TIP4P-Ew. At higher

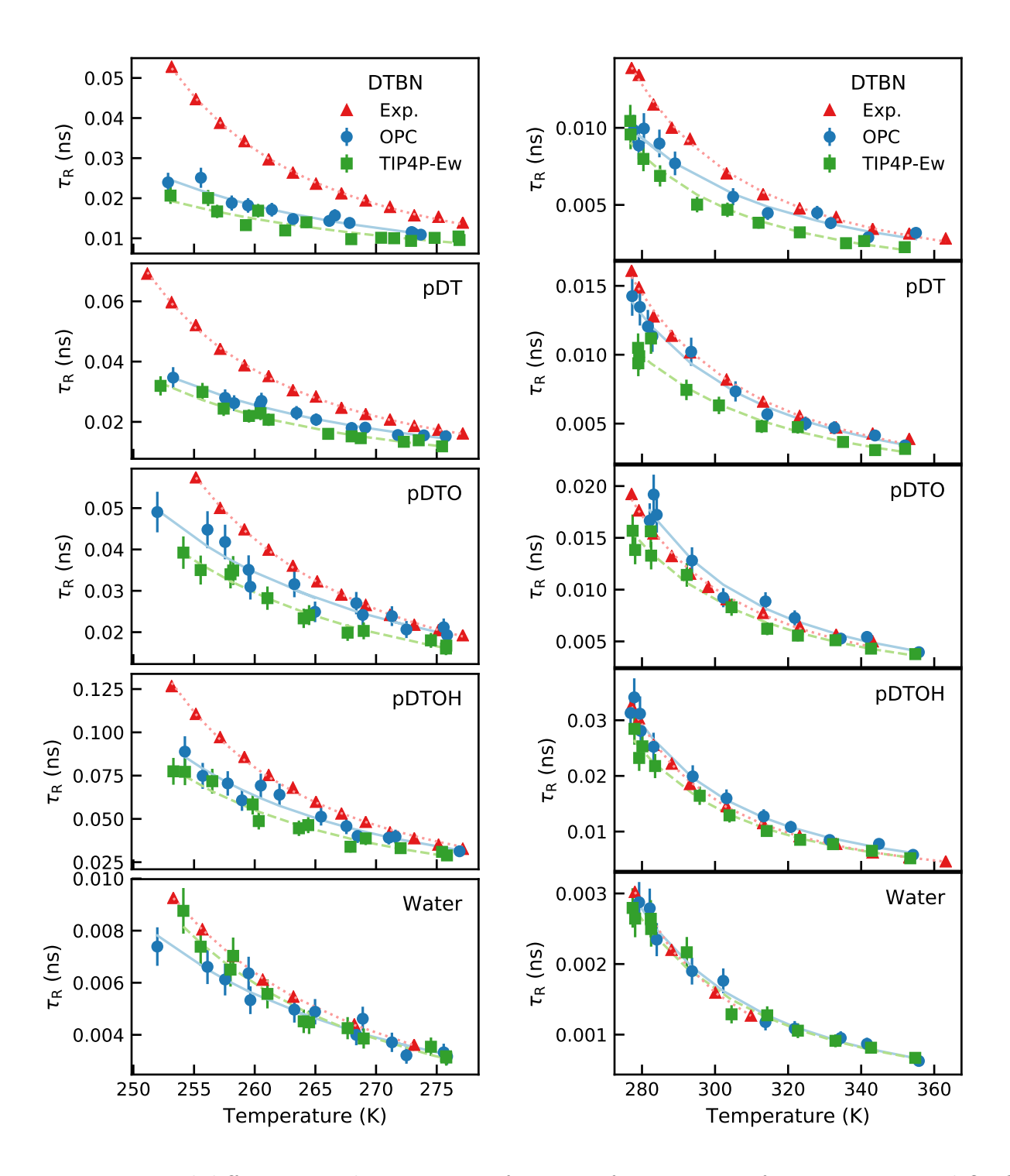


Figure 3: Rotational diffusion correlation time as function of temperature for experiment and OPC and TIP4P-E water models for temperatures (left) below and (right) above 277 K. Data are fit with eq 3 and parameters found in Table 1. Experimental data from ¹⁸.

Table 2: Fit parameters for power law, eq 3, broken up by experiment (top) and simulation (bottom). Standard error in the last digit is given in parentheses. Nitroxide probe and water parameters for experiment are from fits to raw data from Peric et al. ¹⁸ and Qvist et al. ⁴⁸.

Probe	T_0 (K)	$\tau_{R0} \; (\mathrm{ps})$	R^2	T_0 (K)	$\tau_{R0} \; (\mathrm{ps})$	\mathbb{R}^2			
		$T \le 277 \mathrm{K}$			$T \ge 277 \mathrm{K}$				
Experiment									
$\overline{\rm DTBN^{18}}$	228.5(3)	0.61(1)	0.9994	211(2)	1.35(8)	0.9980			
$ m pDT^{18}$	227.2(3)	0.77(2)	0.9993	209(2)	1.6(1)	0.9967			
$ m pDTO^{18}$	225.4(3)	1.00(2)	0.9995	214(2)	1.6(1)	0.995			
$ m pDTOH^{18}$	227.9(5)	1.57(6)	0.9981	225.3(7)	1.72(5)	0.9994			
$Water^{48}$	220.4(3)	0.206(4)	0.9998	219.64(2)	0.2136(2)	1.0000			
			OPC						
DTBN	210(4)	1.0(2)	0.9342	190(7)	2.1(4)	0.9732			
pDT	212(2)	1.3(1)	0.9796	203(3)	1.9(2)	0.9879			
pDTO	212(4)	1.8(3)	0.9419	215(5)	1.7(3)	0.9722			
pDTOH	219(3)	2.2(4)	0.9495	217(2)	2.4(2)	0.9866			
OPC	209(4)	0.39(7)	0.9445	208(4)	0.33(4)	0.9846			
TIP4P-Ew									
DTBN	204(8)	1.1(4)	0.8666	208(5)	1.0(1)	0.9707			
pDT	217(2)	0.9(1)	0.9731	194(6)	1.9(3)	0.9548			
pDTO	215(3)	1.3(2)	0.9733	205(4)	2.0(3)	0.9672			
pDTOH	219(3)	1.9(3)	0.9682	216(2)	2.2(2)	0.9857			
TIP4P-Ew	220(2)	0.20(3)	0.9731	205(4)	0.36(5)	0.9803			

temperatures, the agreement between simulation and experiment is much better. Simulation results for pDTO and pDTOH tightly bracket the experimental results, while OPC results for pDT are in excellent agreement. Again, TIP4P-Ew water gives slightly lower values than OPC throughout and underestimates the experimental result in all cases.

We also compared the rotational diffusion correlation time of water molecules in the simulation to those measured by Qvist et al. 48 (Figures 2 and 3). While the water molecules used for the calculation were taken from the pDT simulations, the large number of water molecules in the simulations means that the selected molecule experiences, on average, a bulk-like environment. Indeed, we observe excellent agreement with experiment across all temperatures. Only at the lowest temperatures does OPC deviate from the experimental data, while TIP4P-Ew is excellent agreement throughout.

To quantitatively assess the agreement between simulation and experiment, we fit the the rotational correlation time, τ_R , with a power-law function of the form

$$\tau_R = \tau_{R0} \left(\frac{T}{T_0} - 1 \right)^{-\gamma}, \tag{3}$$

where T is temperature, and τ_{R0} and T_0 are fit parameters. γ is sometimes treated as a fit parameter but $\gamma = 2$ is used throughout this work. Fit parameters for the full temperature range are given in Table 1 and there is good agreement between the fit function and the experimental data with $R^2 > 0.97$ for almost all of OPC and $R^2 > 0.95$ for TIP4P-Ew. Calculated T_0 for all probe molecules and OPC water are lower than those for the respective experiment. This is consistent with the underestimate of τ_R at low temperatures as the simulations approach a singularity at a slightly lower temperature. Similarly, τ_{R0} is larger for all simulations relative to their respective experiment, except for TIP4P-Ew relative to bulk water.

Simulations were also able to differentiate between the different molecular probes, as demonstrated by the fit values of τ_{R0} (Table 1). For all OPC simulations we observe the molecules may be ordered by τ_{R0} as DTBN \leq pDT < pDTO < pDTOH, just as for experiment. There is some slight ambiguity for TIP4P-Ew, however, as τ_{R0} for DTBN \approx pDT within error. This indicates that DTBN and pDT rotate the fastest while pDTOH is the slowest. Splitting the data into high and low temperatures sets, we observe the same orderings are true in the low temperature data but not the high temperatures data (Table 2). When considering the error in the fit parameters, it is difficult to differentiate between probes for simulation and experiment alike.

 T_0 is often taken as the crossover temperature, T_x , for supercooled water, an approach first proposed by Speedy and Angell¹⁹. For real water, a range of crossover temperatures have been found using this method with different physical parameters. For example, a value of $T_x \approx 228 \,\mathrm{K}$ was determined using isothermal compressibility¹⁹, while more recent rotational diffusion results give a value of $T_x \approx$ 220 K⁴⁸. EPR, averaged over the four probes, gives $T_0 = 226.5 \pm 0.4 \,\mathrm{K}$, well within the range of values determined for pure liquid water. Simulations give slightly lower average crossover temperatures of $T_0 = 212 \pm 2 \,\mathrm{K}$ (OPC) and $T_0 = 215 \pm 2 \,\mathrm{K} \,(\mathrm{TIP4P\text{-}Ew}) \,(\mathrm{Table}\,\,1)$ for the nitroxide probes, which are quite close to the crossover temperatures calculated directly for water of $T_0 = 208 \pm 2 \,\mathrm{K}$ for OPC water and $T_0 = 220 \pm 1 \,\mathrm{K}$ for TIP4P-Ew water. For both simulation and experiment, agreement between water and probe crossover temperatures for simulations is good, despite the fact that the water molecules rotate about 5-10 times faster than the molecular probes at the same temper-

TIP4P-Ew and OPC T_0 values are in good agreement with values for bulk water rotational diffusion data obtained from both experiment and simulations of both models. Demontis et al. ⁴⁹ found a crossover temperature of $T_L = 200 - 203 \,\mathrm{K}$ for TIP4P-Ew, which is found using a different method and is expected to be slightly lower than the singularity temperature found here. Our TIP4P-Ew result agrees particularly well with NMR rotational diffusion ⁴⁸ data, though Qvist et al. use a bi-exponential fit whereas we have used a single-exponential

fit. Note that we refit eq 3 using $\gamma=2$ and only data points from Qvist et al. 48 that match our temperature range, 253 K to 310 K, in order to consistently compare with our results. In a subsequent calculation, Gabrieli et al. 50 found a crossover temperature of $T_L=222\pm5$ K for OPC, which is larger than the value for T_0 we found.

Rotational dynamics of the probe molecule at low temperatures differ significantly from those at high temperatures. After fitting eq 3 separately to each temperature regime (Figure 3 and Table 2), we observe a drop in T_0 and increase in τ_{R0} for almost all probe molecules for high temperatures compared to low. The only exceptions are pDTOH, which has only minor changes in both experiment and simulation, pDTO in OPC water and DTBN in TIP4P-Ew water, for which high and low temperature values are within error of each other. Otherwise, changes in T_0 and τ_{R0} are roughly the same in experiment and simulation for the individual probes. Despite the better agreement between simulation and experimental data, the changes in the fit parameters have some notable differences.

Changes in the quantitative behavior of water at high and low temperatures are not as clear as for the probes. Experimental values of water do not show the same changes in T_0 and τ_{R0} that the probes do; however, we only have four data points from the NMR data, so caution should be used here. OPC water also shows no significant change in fit parameters but TIP4P-Ew experiences a similar shift in T_0 and τ_{R0} , as observed in the probes. In fact, TIP4P-Ew's fit parameters are most similar to real water at low temperatures and most similar to OPC at high temperatures.

Though simulations do capture the apparent change in behavior at low and high temperatures, the visual agreement with experiment is much better at high temperatures than at low. The GAFF, OPC and TIP4P-Ew models are parameterized to be used in room temperature simulations, so it is not surprising that the absolute values above 277 K are in better agreement with experiment but the temperature dependence is not quite correct.

Arrhenius Behavior

Further exploring the apparent change in the behavior of the rotational diffusion correlation time at 277 K, we fit the data to the Arrhenius equation,

$$\tau_R = \tau_{R0} \, e^{\frac{E_A}{RT}} \tag{4}$$

where R is the ideal gas constant and the activation energy, E_A , and τ_{R0} are fit parameters (Figure 4 and Table 3). Water dynamics are known to follow Arrhenius behavior below T_x^{51} and above the temperature of maximum density $T_{\rho_{\text{max}}} = 277 \,\text{K}$ for liquid water. In between, the behavior is super-Arrhenius 52,53 ,

$$\tau_R = \tau_{R0} e^{\frac{E_A}{R(T - T_C)}},$$

though, for water, it is still well approximated by Arrhenius behavior in a narrow temperature interval; here from 253 to 277 K. As density maxima for TIP4p-Ew $(T_{\rho_{\text{max}}} = 274 - 276 \text{ K})^{40,41,50}$ and OPC $(T_{\rho_{\text{max}}} = 272 \pm 1 \text{ K})^{40}$ are close to the value for bulk water, we have used 277 K as the value for T_x for models and experiment.

The rotational diffusion correlation times for the probe molecules from experiment and simulation are well fit by eq 4. Above 277 K, there is good agreement for the activation energies between the simulations and experiment, with values generally close to 16 kJ/mol. The worst agreement is for DTBN, with $E_A = 15.9 \pm$ $0.5 \,\mathrm{kJ/mol}$ from experiment and $E_A = 13 \pm$ 1 kJ/mol from OPC simulation. All other simulation values are very nearly within one standard error of the experimental values, though they tend to be lower than those observed for experiment. Below 277 K, there is substantial disagreement between simulation and experiment. Here, E_A is between $30.9 \pm 0.4 \,\mathrm{kJ/mol}$ and $33.8 \pm 0.3 \,\mathrm{kJ/mol}$ when fit to experiment but only $16 \pm 3 \,\mathrm{kJ/mol}$ and $26 \pm 2 \,\mathrm{kJ/mol}$ when fit to simulation. While the change in activation energy at 277 K is smaller in simulation than experiment, all probes share the same qualitative trend as the experimental results; that is, the activation energies (and therefore slopes) systematically decrease going from below 277 K to above.

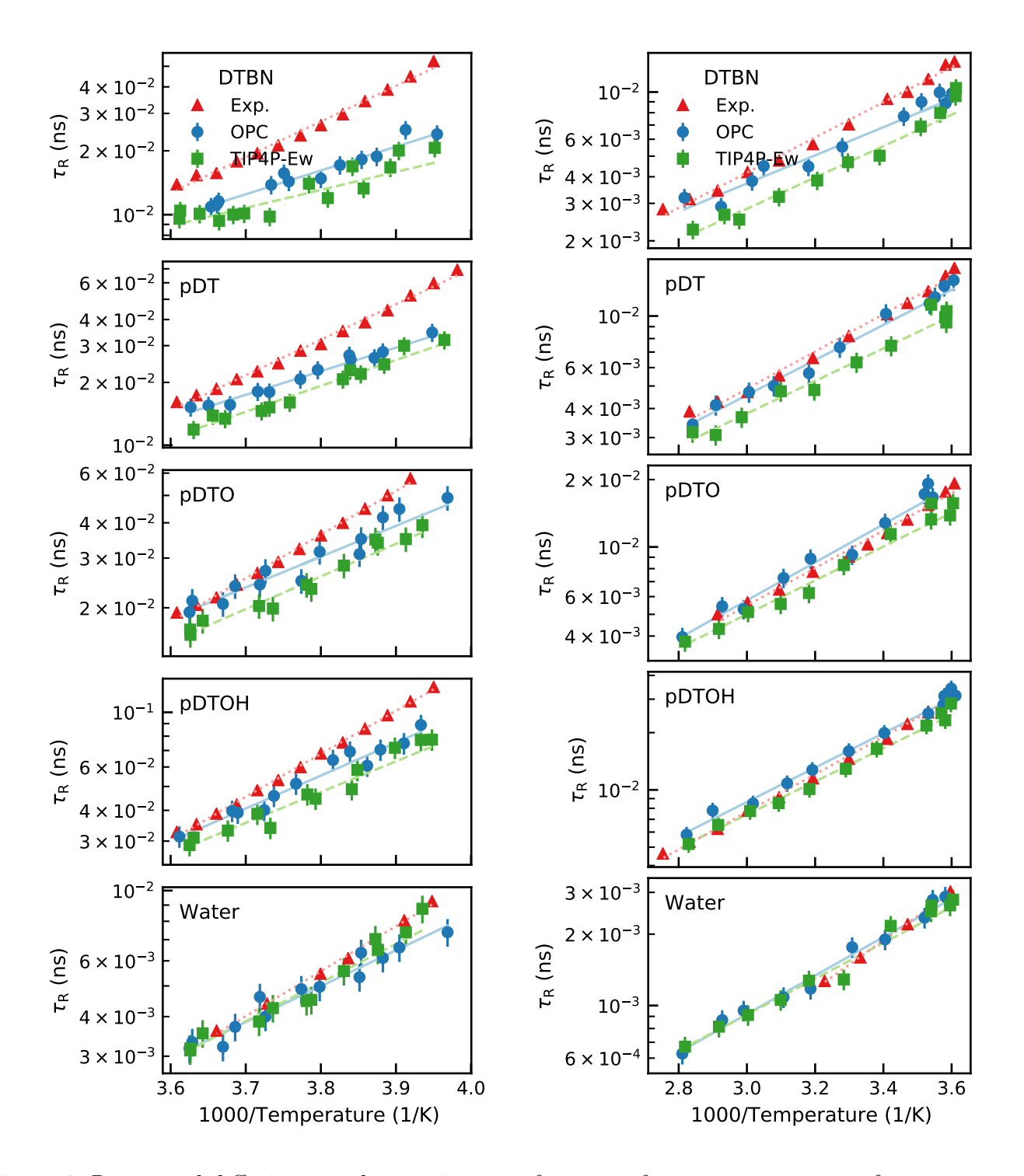


Figure 4: Rotational diffusion correlation time as a function of inverse temperature for experiment and OPC and TIP4P-E water models for temperatures (left) below and (right) above 277 K. Data is fit with eq 4 and parameters can be found in Table 3.

Table 3: Fit parameters for eq 4. The equation was fit independently to simulation and experimental data above and below 277 K. Standard error in the last digit is given in parentheses. Nitroxide probe and water parameters for experiment are from fits to raw data from Peric et al. 18 and Qvist et al. 48.

	$E_A (kJ/mol)$	\mathbb{R}^2	$E_A~(\mathrm{kJ/mol})$	\mathbb{R}^2				
	$T \le 277 \mathrm{K}$		$T \ge 277 \mathrm{K}$					
Experiment								
$\tau_R {\rm DTBN^{18}}$	32.4(8)	0.9970	15.9(5)	0.9654				
$ au_R~{ m pDT^{18}}$	32.7(7)	0.9964	15.7(6)	0.9615				
$ au_R~{ m pDTO^{18}}$	30.9(4)	0.9984	16.1(6)	0.9954				
$ au_R$ pDTOH ¹⁸	33.8(3)	0.9990	19.1(5)	0.9766				
$ au_R ext{ water}^{48}$	27.2(7)	0.9969	19.6(4)	0.9990				
OPC								
DTBN	21(1)	0.9503	13(1)	0.9650				
pDT	22(1)	0.9772	14.5(6)	0.9882				
pDTO	21(2)	0.9360	16.2(9)	0.9785				
pDTOH	26(2)	0.9617	17.3(7)	0.9882				
OPC	22(2)	0.9506	15.5(8)	0.9846				
TIP4P-Ew								
DTBN	16(3)	0.8387	14.1(8)	0.9726				
pDT	24(1)	0.9723	13.4(8)	0.9740				
pDTO	22(1)	0.9691	14.5(7)	0.9820				
pDTOH	24(2)	0.9568	16.7(5)	0.9915				
TIP4P-Ew	23(2)	0.9616	14.5(7)	0.9830				

Quantitative agreement of the water results from simulation and experiment is not as good. Below 277 K, the activation energy for TIP4P-Ew is in good agreement with experiment but is too low for OPC. This is consistent with our power law fit of the data, which showed good agreement between the TIP4P-Ew and experiment but a lower T_0 for OPC. Above 277 K, both OPC and TIP4P-Ew significantly underestimate the activation energy. The overall result is that OPC underestimates the change in activation energy above and below $T_{\rho_{\text{max}}}$ while TIP4-Ew over estimates it. Again, caution should be used for the high temperature NMR rotational diffusion parameters for water as only four data points were available and we used a single-exponential fit for the rotational correlation function instead of a bi-exponential fit used for the NMR data. 48 In all cases, the activation energy for water is similar to that found for the probes and the change in activation energy is about the same.

Hydrogen Bonding

Applying power law and Arrhenius models to the rotational diffusion data shows a strong coupling between probes and the surrounding water. The most likely candidate for this coupling is hydrogen bonding between the probes and water. While we were not able to extract hydrogen bonding information from the experimental data, simulations provide easy access to this information. To identify hydrogen bonding between the probe and water we used the geometric definition of an angle cutoff of 145° and a distance cutoff of 3.5 Å (Theoretical Methods). The defining a hard cut-off for hydrogen bonds is necessarily somewhat arbitrary and, ideally, should vary with temperature. 54-58 However, here, we are using hydrogen bonding semi-quantitatively to gain insight as to the coupling between the nitroxide probes and the surrounding water.

The number of hydrogen bonds, $N_{\text{H-Bond}}$, as function of temperature for each probe molecule is given in Figure 5. Notably, the relationship between $N_{\text{H-Bond}}$ and temperature is nearly linear and, with the exception of pDT, and pDTO

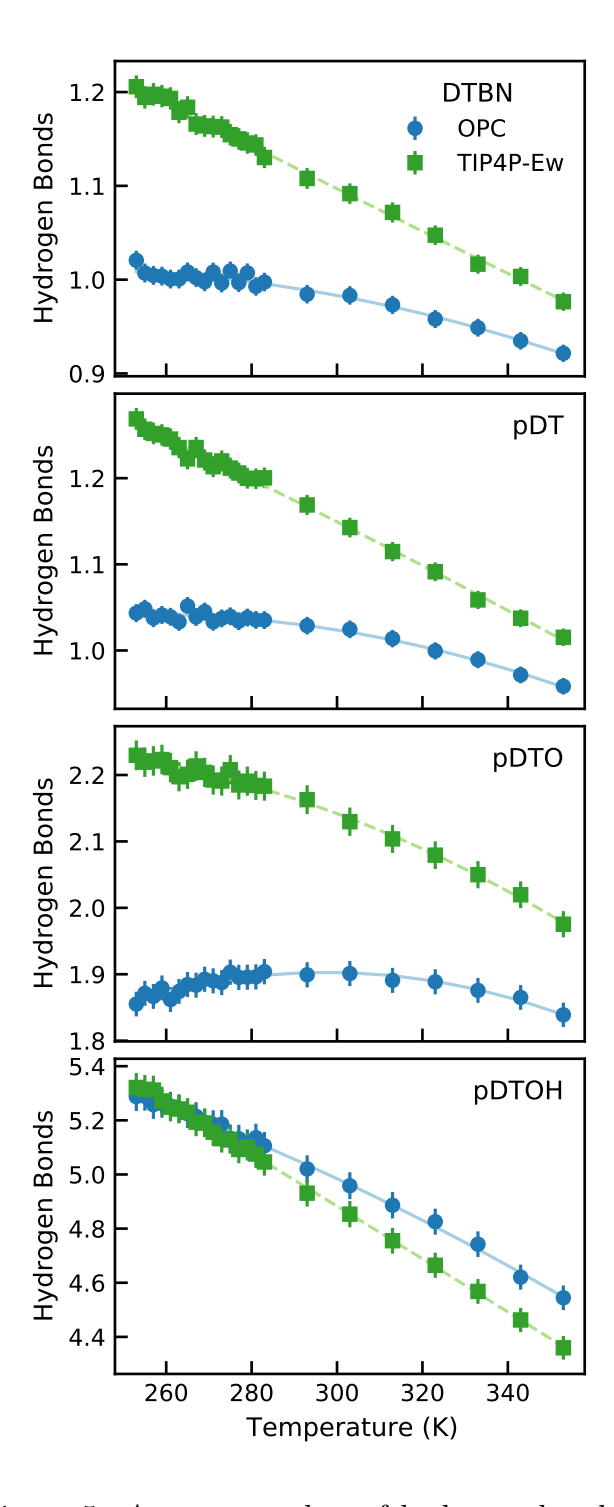


Figure 5: Average number of hydrogen bonds between the probe and surrounding water as a function of temperature.

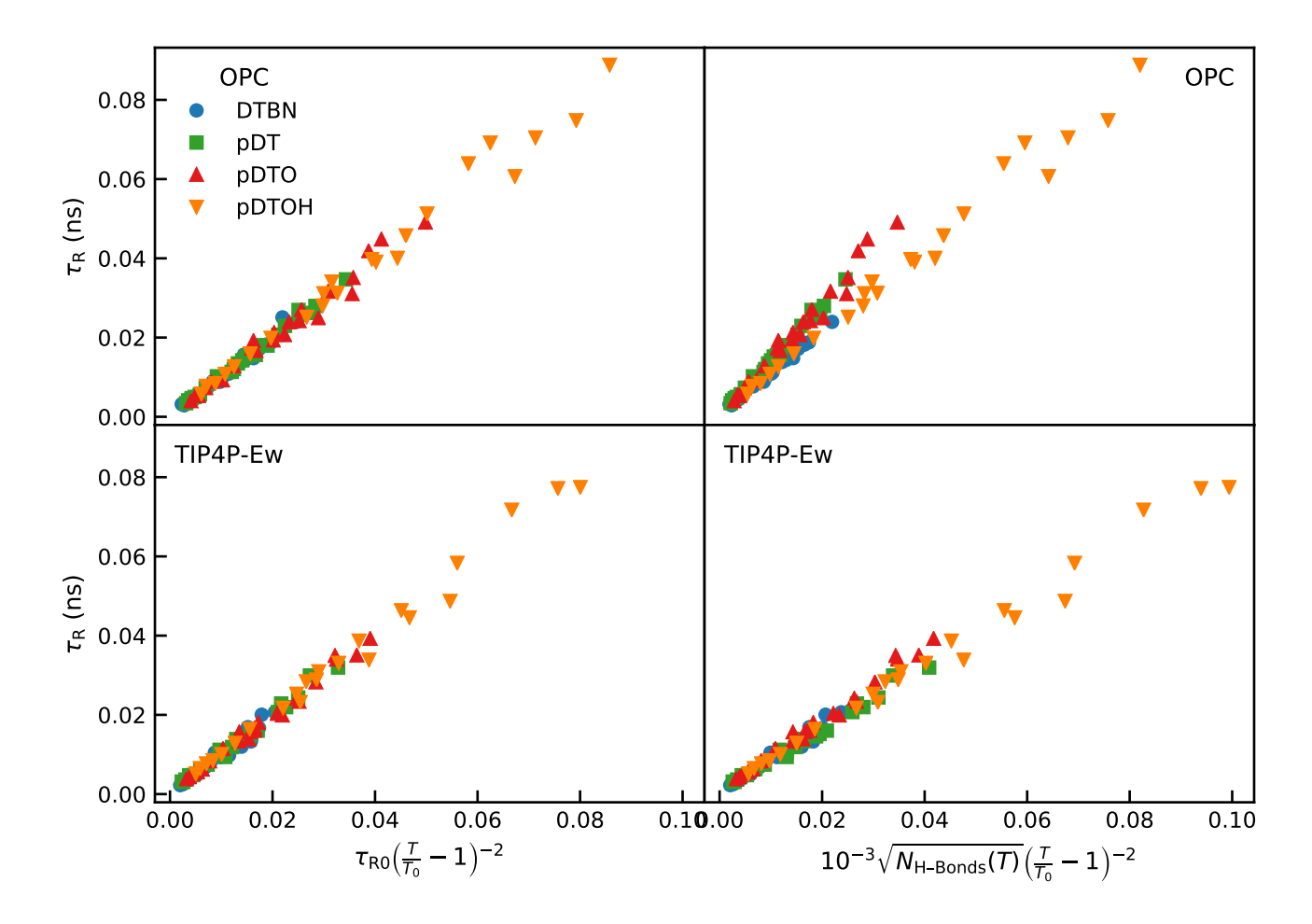


Figure 6: Power law behavior of τ_R . (Left) τ_R vs. the left-hand-side of eq 3, using fitting parameters from Table 1. (Right) τ_R vs. the left-hand-side of eq 3, using $\tau_{R0} = (10^{-3} \text{ ns}) \sqrt{N_{\text{H-Bonds}}(T)}$ for all probe molecules.

in OPC, show little sign of saturating at the lowest temperatures. Data was fit with a simple quadratic polynomial,

$$N_{\text{H-Bonds}}(T) = c_0 + c_1 T + c_2 T^2,$$

where c_0 , c_1 , and c_2 are fit coefficients. While we are able to do high quality fits ($R^2 > 0.99$), extrapolating to a maximum value yields non-sensical results.

From Figure 5 we also observe that probe molecules with more hydrogen bonds have longer τ_R . In fact, the ratios of τ_{R0} in Table 1 are very close to the ratios of the square roots of $N_{\text{H-Bond}}(T)$. In Figure 6, we plot τ_R against the left-hand-side of eq 3, using fit parameters from Table 1 and using $\tau_{R0} \approx$ $(10^{-3} \text{ ns}) N_{\text{H-Bonds}}(T)$ for all probe molecules. For both OPC and TIP4P-Ew, replacing the fit τ_{R0} with the $N_{\text{H-Bonds}}(T)$ based value provides nearly identical results. This does work better for TIP4P-Ew than OPC; the largest deviation from the numerical fit is for pDT and pDTO in OPC water, which also show the most pronounced non-linearity in Figure 5. This may be due to the geometric definition of hydrogen bonds and slight differences in the models. It is worth noting that the temperature dependence of $N_{\text{H-Bonds}}$ does not matter much, as there is only a small change in the given temperature range. For example, using the maximum observed number of hydrogen bonds works just as well (data not shown).

From this, we conclude that hydrogen boding explains almost all variation between the probe molecules. Figure 6 is still using the fit values for T_0 , which are slightly different between the probe molecules. In addition, we are unable to address the role of size as the volume of each of the molecules is almost the same. Other contributing factors include the solvent used and van der Waals interactions, which are negligible compared to hydrogen bonding.

Discussion

Effects of Water Models

The water models used in this study are fixedcharge, 4-point models with similar parameters but still yield systematic differences in the observed results. TIP4P-Ew⁴¹ is a reparameterization of the TIP4P water model⁵⁹ for use with Ewald summation electrostatics. OPC is a relatively new refinement of the 4point model where the geometry of the molecule was optimized in addition to partial charges and Lennard-Jones parameters. 40 TIP4P-Ew is a widely used and well-characterized model while OPC is less studied but should be a more accurate model of bulk water. Both models reproduce experimental bulk density, heat of vaporization, and self diffusion coefficient well over the range of temperatures considered here. 40 OPC additionally provides static dielectric coefficients, isobaric heat capacities, and isothermal compressibilities in good agreement with experiment while TIP4P-Ew does not.

Based on both power law and Arrhenius behavior, TIP4P-Ew is in better agreement with experiment for both bulk water rotational diffusion correlation times and crossover temperatures. This is particularly evident at low temperatures, where TIP4P-Ew remains in good agreement with experimental results while OPC diverges. The reasons for this are not clear, considering that OPC performs as well as or better than TIP4P-Ew for a variety of other bulk properties.

Differences between the water models for the rotational diffusion correlation times of molecular probes are smaller than for the water models themselves. Both models tend to underestimate the correlation times, particularly at low temperatures. This suggests that the simulation probes are not interacting strongly enough with the water models, which has been observed for proteins, small molecules, and ions. ^{60–62} In particular, Nerenberg et al. ⁶¹ found that solvation free energies calculated with the GAFF force field and TIP4P-Ew were too high compared to experiment. By modifying the Lennard-Jones interaction parameters between the solutes and

water, both mean signed and root mean squared errors were greatly reduced. Several of these modifications strengthened hydrogen bonding between the solute and water. Applying such modifications to the probe molecules in this study could potentially increase the strength of hydrogen bonds with the water and increase rotational diffusion correlation times. We would expect the effect to be more pronounced at low temperatures, where reduced thermal fluctuations would allow for longer and closer hydrogen bonds. TIP4P-Ew shows a consistently higher number of hydrogen bonds with the probes than OPC. Though the difference is small, the consistency across models and temperatures suggests that it is not a statistical artifact. However, probes in OPC tend to rotate slower and are, therefore, in better agreement with experimental data. One possibility is that the OPC model permits hydrogen bonds at larger angles that are missed by the cutoff in the geometric definition.

Temperature Dependence

Near the temperature of maximum water density, $T_{\rho_{\text{max}}}$, there is distinct change in the Arrhenius behavior, eq 4, of probe and water rotational diffusion correlation times. In both experiment and simulation, the activation energy drops when the temperature is raised above $T_{\rho_{\text{max}}}$. At high temperatures, the agreement between simulation and experiment activation energies is good. However, at low temperatures, the activation energy of the probes measured from experiment is much larger than that measured for water or any of the models. The result is that the change in the activation energy is much larger for the experimental probes than for water, an effect that is not captured by simulation. A possible reason is that at low temperatures the probes interact with water much more strongly and the relatively weaker interactions of the models does not experiences as large a change. As discussed previously, a solution to this may be to modify the Lennard-Jones parameters of the GAFF force field and strengthen the hydrogen bonding between the probes and water.

However, when we apply a power-law model, eq 3, the change in behavior at $T_{\rho_{\text{max}}}$ is not as clear. Results from experiment show T_0 dropping and τ_{R0} increasing for DTBN, pDT, and pDTO when going from low to high temperatures. However, pDTOH and water show only very small changes in these same parameters. A similar situation is observed when we consider the models. Both models show a negligible shift for pDTOH. OPC water also has a negligible shift but TIP4P-Ew does have a significant change in parameters. DTBN, pDT and pDTO mostly experience shifts similar to experiment but DTBN in TIP4P-Ew shifts in the opposite direction and pDTO in OPC has no change within error.

Conclusion

To investigate the diffusive behavior of supercooled water, we did 200 ns MD simulations of four nitroxide probes at twenty-three temperatures. Trajectories of the probes were analyzed for rotational correlation times and hydrogen bonding between the probes and water. As far as we know, this work is the first one in which rotational diffusion EPR experiments are compared with MD simulations.

We found that simulations were able to reproduce the observed rotational diffusion correlation times of the probes from experiments, though results above 277 K were quantitatively in better agreement. Below 277 K, simulations generally had faster rotational diffusion than observed in experiment while above 277 K, agreement was quite good.

Fitting the simulation data with the power law and Arrhenius equations provided R^2 values all above 0.9 except for one low-temperature case. From these fits, we were able to calculate power law singularities near the cross over temperature of 228 K, rotational diffusion constants, and activation energies of the probe molecules. The crossover temperatures of the models were about 10 K lower than experiment, consistent with the behavior of the water models used. We were also able to rank the probes by rotational diffusion correlation coefficients

from the power-law consistent with experiment, DTBN \leq pDT < pDTO < pDTOH. Activation energies of the probes above 277 K are significantly smaller than those below 277 K. However, while activation energies above 277 K were in excellent agreement with experiment, activation energies below 277 K were underestimated in the simulations, consistent with the faster rotational diffusion times observed at these temperatures. This indicates that the change in behavior at 277 K still occurs in the water models but is less profound.

To understand why the probes exhibit different behavior, we examined hydrogen bonding between the probes and surrounding water. As expected, both lower temperatures and more hydrogen bond acceptors and donors of the probe molecules increased the amount of hydrogen bonding that occurs. Indeed, we found that the ranking of probe molecules by the number of hydrogen bonds was consistent with ranking by rotational diffusion correlation coefficients: DTBN < pDT < pDTO < pDTOH. Furthermore, we were able to show that the number of hydrogen bonds between the probe and surrounding water was sufficient to explain differences in rotational diffusion correlation coefficients of the probes.

In future work, we plan to extend this approach to other liquids that exhibit supercooled behavior, such as room temperature ionic liquids. **Acknowledgement** TL was supported by the National Science Foundation (NSF) under Grant 1566638 and the Research Corporation for Science Advancement (RCSA) Cottrell Scholar Award 23967. M.P. gratefully acknowledges support from NSF MRI Grant 1626632 and NSF RUI 1856746.

References

- (1) Alberts, B., Ed. Molecular biology of the cell, 3rd ed.; Garland Pub: New York, 1994.
- (2) Saha, R.; Pohorille, A.; Chen, I. A. Molecular crowding and early evolution. *Origins*

- of Life and Evolution of Biospheres **2015**, 44, 319–324.
- (3) Debenedetti, P. G. Supercooled and glassy water. *Journal of Physics: Condensed Matter* **2003**, *15*, R1669–R1726.
- (4) Debenedetti, P. G.; Stanley, H. E. Supercooled and glassy water. *Physics Today* **2003**, *56*, 40–46.
- (5) Pettersson, L. G. M.; Henchman, R. H.; Nilsson, A. Water—the most anomalous liquid. *Chemical Reviews* **2016**, *116*, 7459–7462, Publisher: American Chemical Society.
- (6) Rosenfeld, D.; Woodley, W. L. Deep convective clouds with sustained supercooled liquid water down to -37.5°C. *Nature* **2000**, 405, 440–442.
- (7) Sellberg, J. A.; Huang, C.; Mc-Queen, T. A.; Loh, N. D.; Laksmono, H.; Schlesinger, D.; Sierra, R. G.; Nordlund, D.; Hampton, C. Y.; Starodub, D. et al. Ultrafast X-ray probing of water structure below the homogeneous ice nucleation temperature. *Nature* **2014**, 510, 381–384.
- (8) Lowe, C. H.; Lardner, P. J.; Halpern, E. A. Supercooling in reptiles and other vertebrates. Comparative Biochemistry and Physiology Part A: Physiology 1971, 39, 125–135.
- (9) Angell, C. A. Insights into phases of liquid water from study of its unusual glass-forming properties. *Science* **2008**, *319*, 582–587.
- (10) Teixeira, J. Recent experimental aspects of the structure and dynamics of liquid and supercooled water. *Molecular Physics* 2012, 110, 249–258.
- (11) Mishima, O.; Stanley, H. E. The relationship between liquid, supercooled and glassy water. *Nature* **1998**, *396*, 329–335.

- (12) Banerjee, D.; Bhat, S. N.; Bhat, S. V.; Leporini, D. ESR evidence for 2 coexisting liquid phases in deeply supercooled bulk water. Proceedings of the National Academy of Sciences 2009, 106, 11448– 11453.
- (13) Bhat, S. N.; Sharma, A.; Bhat, S. V. Vitrification and glass transition of water: insights from spin probe ESR. *Physical Review Letters* **2005**, *95*, 235702.
- (14) Banerjee, D.; Bhat, S. N.; Bhat, S. V.; Leporini, D. Molecular probe dynamics reveals suppression of ice-like regions in strongly confined supercooled water. *PLoS ONE* **2012**, *7*, e44382.
- (15) Floridi, G.; Lamanna, R.; Cannistraro, S. Rotational dynamics of Di-tert-butyl-nitroxide in normal and supercooled water: an electron paramagnetic resonance study. *Applied Magnetic Resonance* **1994**, 7, 537–550.
- (16) Ahn, M.-K. Electron spin relaxation of di-tertiary-butyl nitroxide in supercooled water. *The Journal of Chemical Physics* **1976**, *64*, 134–138.
- (17) Santangelo, M. G.; Levantino, M.; Cupane, A.; Jeschke, G. Solvation of a Probe Molecule by Fluid Supercooled Water in a Hydrogel at 200 K. The Journal of Physical Chemistry B 2008, 112, 15546–15553.
- (18) Peric, I.; Merunka, D.; Bales, B. L.; Peric, M. Rotation of four small nitroxide probes in supercooled bulk water. *The Journal of Physical Chemistry Letters* **2013**, 4, 508–513.
- (19) Speedy, R. J.; Angell, C. A. Isothermal compressibility of supercooled water and evidence for a thermodynamic singularity at -45°C. The Journal of Chemical Physics 1976, 65, 851–858.
- (20) Chen, S.-H.; Gallo, P.; Sciortino, F.; Tartaglia, P. Molecular-dynamics study of incoherent quasielastic neutron-scattering

- spectra of supercooled water. *Physical Review E* **1997**, *56*, 4231–4243.
- (21) Peric, I.; Merunka, D.; Bales, B. L.; Peric, M. Hydrodynamic and nonhydrodynamic contributions to the bimolecular collision rates of solute molecules in supercooled bulk water. *The Journal of Physical Chemistry B* **2014**, *118*, 7128–7135.
- (22) Gallo, P.; Sciortino, F.; Tartaglia, P.; Chen, S.-H. Slow Dynamics of Water Molecules in Supercooled States. *Physical Review Letters* 1996, 76, 2730–2733.
- (23) Qvist, J.; Schober, H.; Halle, B. Structural dynamics of supercooled water from quasielastic neutron scattering and molecular simulations. *The Journal of Chemical Physics* **2011**, *134*, 144508.
- (24) Sciortino, F.; Gallo, P.; Tartaglia, P.; Chen, S. H. Supercooled water and the kinetic glass transition. *Physical Review E* **1996**, *54*, 6331–6343.
- (25) Merunka, D.; Peric, M. Continuous diffusion model for concentration dependence of nitroxide epr parameters in normal and supercooled water. *The Journal of Physical Chemistry B* **2017**, *121*, 5259–5272.
- (26) Berliner, L. J. Spin labeling: theory and applications.; Academic Press, Inc.: New York, 1976; OCLC: 1039718100.
- (27) Merunka, D.; Peric, M.; Peric, M. Study of nanostructural organization of ionic liquids by electron paramagnetic resonance spectroscopy. *The Journal of Physical Chemistry B* **2015**, *119*, 3185–3193.
- (28) Salomon-Ferrer, R.; Case, D. A.; Walker, R. C. An overview of the Amber biomolecular simulation package. Wiley Interdisciplinary Reviews: Computational Molecular Science 2013, 3, 198–210.
- (29) Case, D. A.; Betz, R. M.; Cerutti, D. S.; T.E. Cheatham, I. I. I.; Darden, T. A.; Duke, R. E.; Giese, T. J.; Gohlke, H.;

- Goetz, A. W.; Homeyer, N. et al. AMBER 2016 reference manual. 2016.
- (30) Wong, V.; Case, D. A. Evaluating rotational diffusion from protein MD simulations. *The Journal of Physical Chemistry B* **2008**, *112*, 6013–6024.
- (31) Allnér, O.; Foloppe, N.; Nilsson, L. Motions and entropies in proteins as seen in NMR relaxation experiments and molecular dynamics simulations. *The Journal of Physical Chemistry B* **2014**, *119*, 1114–1128.
- (32) Zerbetto, M.; Polimeno, A.; Meirovitch, E. General theoretical/computational tool for interpreting NMR spin relaxation in proteins. *The Journal of Physical Chemistry B* **2009**, *113*, 13613–13625.
- (33) Chen, K.; Tjandra, N. Extended model free approach to analyze correlation functions of multidomain proteins in the presence of motional coupling. *Journal of the American Chemical Society* **2008**, *130*, 12745–12751.
- (34) Wang, J.; Wolf, R. M.; Caldwell, J. W.; Kollman, P. A.; Case, D. A. Development and testing of a general amber force field. *Journal of Computational Chemistry* **2004**, *25*, 1157–1174.
- (35) Frisch, M. J.; Trucks, G. W.; Schlegel, H. B.; Scuseria, G. E.; Robb, M. A.; Cheeseman, J. R.; Scalmani, G.; Barone, V.; Petersson, G. A.; Nakatsuji, H. et al. Gaussian 09.
- (36) Bayly, C. I.; Cieplak, P.; Cornell, W.; Kollman, P. A. A well-behaved electrostatic potential based method using charge restraints for deriving atomic charges: the RESP model. *The Journal of Physical Chemistry* **1993**, *97*, 10269–10280.
- (37) Dupradeau, F.-Y.; Pigache, A.; Zaffran, T.; Savineau, C.; Lelong, R.; Grivel, N.; Lelong, D.; Rosanski, W.; Cieplak, P. The R.E.D. tools: advances in RESP and ESP charge derivation

- and force field library building. *Physical Chemistry Chemical Physics* **2010**, *12*, 7821–7839.
- (38) Wang, F.; Becker, J.-P.; Cieplak, P.; Dupradeau, F.-Y. R.E.D. Python: Object oriented programming for Amber force fields. 2013.
- (39) Vanquelef, E.; Simon, S.; Marquant, G.; Garcia, E.; Klimerak, G.; Delepine, J. C.; Cieplak, P.; Dupradeau, F.-Y. R.E.D. Server: a web service for deriving RESP and ESP charges and building force field libraries for new molecules and molecular fragments. *Nucleic Acids Research* **2011**, 39, W511–W517.
- (40) Izadi, S.; Anandakrishnan, R.; Onufriev, A. V. Building water models: a different approach. *The Journal of Physical Chemistry Letters* **2014**, 5, 3863–3871.
- (41) Horn, H. W.; Swope, W. C.; Pitera, J. W.; Madura, J. D.; Dick, T. J.; Hura, G. L.; Head-Gordon, T. Development of an improved four-site water model for biomolecular simulations: TIP4P-Ew. The Journal of Chemical Physics 2004, 120, 9665–9678.
- (42) Liu, D. C.; Nocedal, J. On the limited memory BFGS method for large scale optimization. *Mathematical Programming* **1989**, 45, 503–528.
- (43) Salomon-Ferrer, R.; Götz, A. W.; Poole, D.; Le Grand, S.; Walker, R. C. Routine Microsecond Molecular Dynamics Simulations with AMBER on GPUs. 2. Explicit Solvent Particle Mesh Ewald. Journal of Chemical Theory and Computation 2013, 9, 3878–3888.
- (44) Ryckaert, J.-P.; Ciccotti, G.; Berendsen, H. J. C. Numerical integration of the cartesian equations of motion of a system with constraints: molecular dynamics of n-alkanes. *Journal of Computational Physics* **1977**, *23*, 327–341.

- (45) Darden, T.; York, D.; Pedersen, L. Particle mesh Ewald: An N.log(N) method for Ewald sums in large systems. *The Journal of Chemical Physics* **1993**, *98*, 10089–10092.
- (46) Lajzerowicz-bonneteau, J. In Spin Labeling; Berliner, L. J., Ed.; Molecular Biology: An International Series of Monographs and Textbooks; Academic Press: Amsterdam, 1976; pp 239–249.
- (47) Roe, D. R.; Cheatham, T. E. PTRAJ and CPPTRAJ: software for processing and analysis of molecular dynamics trajectory data. *Journal of Chemical Theory and Computation* **2013**, *9*, 3084–3095.
- (48) Qvist, J.; Mattea, C.; Sunde, E. P.; Halle, B. Rotational dynamics in supercooled water from nuclear spin relaxation and molecular simulations. *The Journal of chemical physics* **2012**, *136*, 204505.
- (49) Demontis, P.; Gulín-González, J.; Masia, M.; Sant, M.; Suffritti, G. B. The interplay between dynamic heterogeneities and structure of bulk liquid water: A molecular dynamics simulation study. *The Journal of Chemical Physics* **2015**, *142*, 244507.
- (50) Gabrieli, A.; Sant, M.; Izadi, S.; Shabane, P. S.; Onufriev, A. V.; Suffritti, G. B. High-temperature dynamic behavior in bulk liquid water: A molecular dynamics simulation study using the OPC and TIP4P-Ew potentials. Frontiers of Physics 2018, 13, 138203.
- (51) Picasso, G. C.; Malaspina, D. C.; Carignano, M. A.; Szleifer, I. Cooperative dynamic and diffusion behavior above and below the dynamical crossover of supercooled water. *The Journal of Chemical Physics* **2013**, *139*, 044509.
- (52) Liu, L.; Chen, S.-H.; Faraone, A.; Yen, C.-W.; Mou, C.-Y. Pressure dependence of fragile-to-strong transition and a possible second critical point in supercooled

- confined water. *Physical Review Letters* **2005**, *95*, 117802.
- (53) Bagchi, B. Water in biological and chemical processes: from structure and dynamics to function; Cambridge molecular science; Cambridge University Press: Cambridge, 2013.
- (54) Ozkanlar, A.; Zhou, T.; Clark, A. E. Towards a unified description of the hydrogen bond network of liquid water: A dynamics based approach. *The Journal of Chemical Physics* **2014**, *141*, 214107, Publisher: American Institute of Physics.
- (55) Prada-Gracia, D.; Shevchuk, R.; Rao, F. The quest for self-consistency in hydrogen bond definitions. The Journal of Chemical Physics 2013, 139, 084501, Publisher: American Institute of Physics.
- (56) Kumar, R.; Schmidt, J. R.; Skinner, J. L. Hydrogen bonding definitions and dynamics in liquid water. The Journal of Chemical Physics 2007, 126, 204107, Publisher: American Institute of Physics.
- (57) Dočkal, J.; Svoboda, M.; Lísal, M.; Moučka, F. A general hydrogen bonding definition based on three-dimensional spatial distribution functions and its extension to quantitative structural analysis of solutions and general intermolecular bonds. *Journal of Molecular Liquids* **2019**, 281, 225–235.
- (58) Galicia-Andrés, E.; Dominguez, H.; Pizio, O. Temperature dependence of the microscopic structure and density anomaly of the SPC/E and TIP4P-Ew water models. Molecular dynamics simulation results. *Condensed Matter Physics* **2015**, *18*, 13603, arXiv: 1504.01217.
- (59) Jorgensen, W. L.; Chandrasekhar, J.; Madura, J. D.; Impey, R. W.; Klein, M. L. Comparison of simple potential functions for simulating liquid water. *The Journal* of Chemical Physics 1983, 79, 926–935.

- (60) Robustelli, P.; Piana, S.; Shaw, D. E. Developing a molecular dynamics force field for both folded and disordered protein states. *Proceedings of the National Academy of Sciences* **2018**, *115*, E4758–E4766.
- (61) Nerenberg, P. S.; Jo, B.; So, C.; Tripathy, A.; Head-Gordon, T. Optimizing solute—water van der waals interactions to reproduce solvation free energies. *The Journal of Physical Chemistry B* **2012**, 116, 4524–4534.
- (62) Joung, I. S.; Cheatham, T. E. Determination of Alkali and Halide Monovalent Ion Parameters for Use in Explicitly Solvated Biomolecular Simulations. *The Journal of Physical Chemistry B* **2008**, *112*, 9020–9041.

Graphical TOC Entry

